Boosting microparticle tracking with neuromorphic cameras by optical modulation

José Huenchual-Escobar[1], Pablo Solano[1], J. Pablo Staforelli V.[1], Esteban Vera R.[2], and Jorge Tapia F.[3,*]

[1]Universidad de Concepción, Facultad de Ciencias Físicas y Matemáticas, Departamento de Física, Concepción, 4070386, Chile
[2]School of Electrical Engineering, Pontificia Universidad Católica de Valparaíso, Brasil 2147, Valparaíso, 2362804, Chile
[3]Departamento de Física, Universidad Técnica Federico Santa María, Av. España 1680, Valparaíso, 2390123, Chile
[*]Corresponding Author: jorge.tapiaf@usm.cl

Supplementary Note 1: Dynamic viscosity of water

The equations used to calculate the viscosity of water $(kg/m \cdot s)$ were obtained from the CRC Handbook of Chemistry and Physics, 69th edition.[1]. The equations are as follows:

$$\eta_{\text{water}}(T) = \begin{cases} 10^{-3}(10^{A(T)}), \text{ for } 0 < T < 20°\text{C} \\ 1.002 \cdot 10^{-3}(10^{B(T)}), \text{ for } 20 < T < 100°\text{C} \end{cases} \tag{1}$$

where,

$$A(T) = \frac{1301}{a + b(T-20) + c(T-20)^2} - 1.30223, \tag{2}$$

$$B(T) = \frac{1.3272(20-T) - 0.001053(T-20)^2}{T+105}, \tag{3}$$

with $a = 998.333$, $b = 8.1855$ and $c = 0.00585$.

Note that the expression for viscosity below 20°C comes from the work of Hardy and Cottington[2], while that for temperatures over 20°C was proposed by Swindells et al.[3].

Supplementary Note 2: Individual diffusion measures distribution

As we point out in the main text, 672 individual diffusion estimations were made, each one with a different 3-second clip. Then, they were grouped by temperature to use the main value of each set as the representative estimation for the diffusion coefficient. This value, along with the standard error of the mean, is presented and discussed.

Additional information about the values distribution for each set is included in figure 1, here the mean values with error bars are replaced by box plots. A box plot displays the distribution of a data set through its quartiles. The box represents the interquartile range (IQR), with its edges marking the first (Q1) and third quartiles (Q3). The lines that exit the box are called Whiskers and extend from the box to the smallest and largest values within 1.5 × IQR of the edges of the box. The lines inside the box represent the median of the set, and a marker (circle or square) represents the mean value for comparison. Figure 1 is composed of two panels, each having the diffusion values obtained from the x or y component of the trajectories.

The diffusion coefficient is obtained from the slope of the mean square displacement curve, with the x (blue circles) and y (orange squares) components analyzed separately. Each marker denotes the mean value of D from all 3-second clips within a 4°C temperature bin, and the error bars represent the standard error of the mean.

Supplementary Note 3: Diffusion coefficient near a wall

The diffusion coefficient of a spherical particle near a wall is given by a modified Stokes-Einstein-Sutherland equation due to hydrodynamic interactions with the boundary. This effect reduces the mobility of the particle, decreasing the value for the

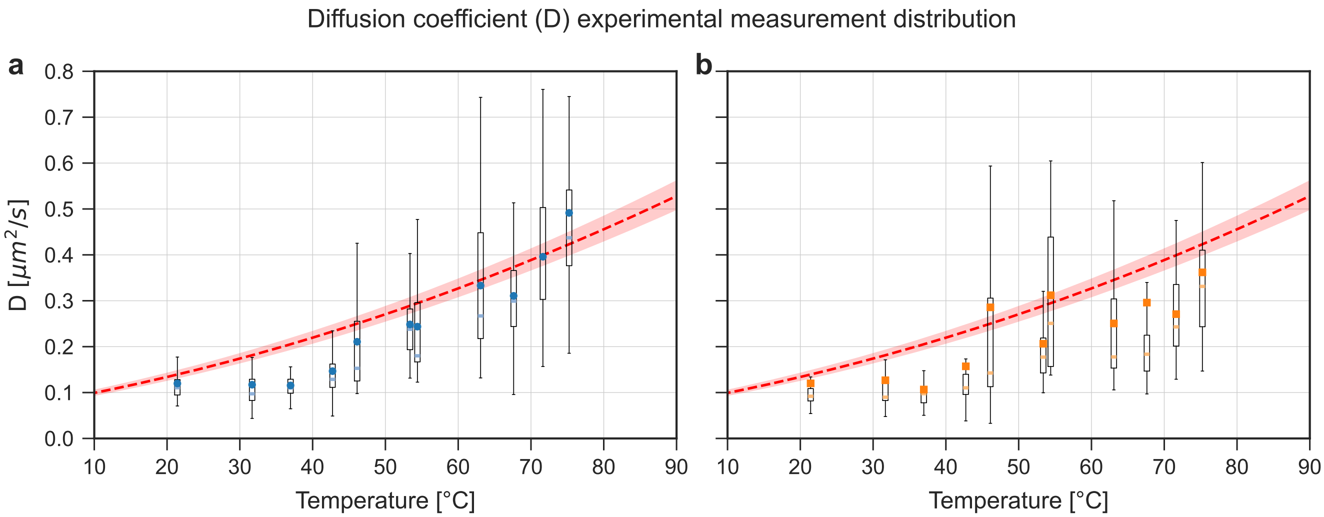

Figure 1. Box plot representation of the diffusion coefficient estimations. The values from the phenomenological model for particles with a radii of 1.6 μm are represented by a red dashed line, while the colored confidence region reflects an uncertainty of 0.095 μm in the particle radii. (a) Diffusion coefficients from the x component of the particles trajectories. Each box represent the distribution of values for a 4°C window, centered at the mean value of the temperature for said set. The line inside the box represent the median of the set while the circle marker represent the mean value. (b) Similar to the first panel, but these diffusion coefficients are obtained from the y component of the particles trajectories, and an square marker represent the mean value.

diffusion coefficient across all temperatures by a multiplicative factor, the exact value of this coefficient depends on the distance to the wall, and has different behaviors depending if the diffusion is normal or parallel to the wall. For a particle of radius r at a distance h from the wall to the nearest border of the particle, the corrected parallel diffusion coefficient is given by

$$D_{\|} = \frac{k_B T}{6\pi r \eta} \cdot C_{\|}$$

where

$$C_{\|} = 1 - \frac{9}{16}\alpha + \frac{1}{8}\alpha^3 - \frac{45}{256}\alpha^4 - \frac{1}{16}\alpha^5$$

and $\alpha = (1 + h/r)^{-1}$.

This correction is derived from hydrodynamic theory being first presented in the works of Lorentz[4] and Faxen[5], a more in detail presentation of the modifications to diffusion coefficients near a wall can be found in the work of Reinhardt et al.[6].

Supplementary Methods 1: How events are processed

Figure 2 illustrates the process of converting events into positions. The EBC records events, which are stored as a list where each event is represented by four values: coordinates x and y, the polarity of the event and the timestamp. The coordinates x and y are integers ranging from 0 to 639 and 0 to 479, respectively, representing the pixel positions where the event was detected. The polarity is a binary value that indicates whether the event signifies an increase or decrease in the intensity of the pixel. The timestamp denotes the time at which the event was detected and is saved as an integer value representing the time in microseconds since the recording began.

After importing the list of events as a dataframe, the data is processed to determine the particle's position. The first step is to group the events into segments based on a predefined acquisition time, t_{acq}. All events contained in a segment are used to estimate a single point in the trajectory of the particle. To obtain this point, the events of the segment are separated by polarity, and for each polarity, the positions X_p and Y_p are calculated as the median of the values x and y. The final position of the particle is then determined as the mean of the X_p and Y_p positions.

The final error value for position due to the algorithm is calculated as the propagation of the standard error of the median.

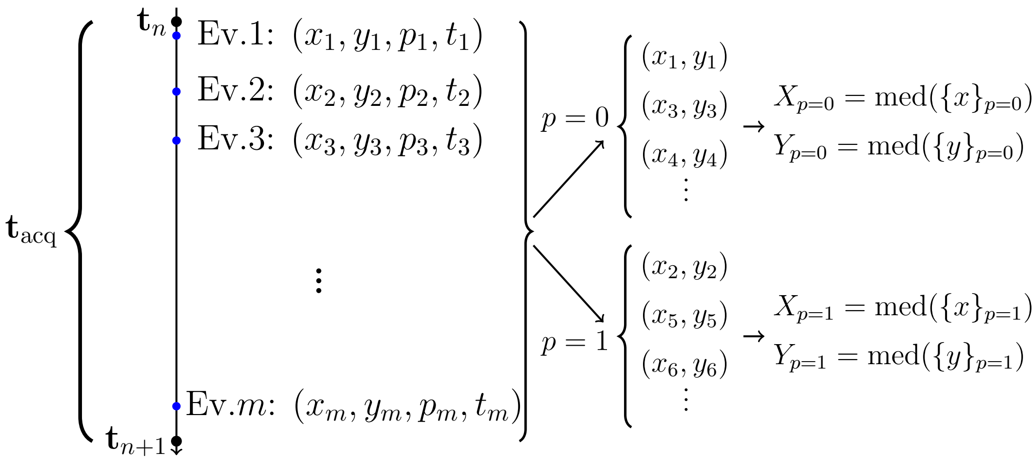

Figure 2. Events processing algorithm diagram. A visualization of how events are processed to obtain the position of the center of the particle.

Being $\text{SE}_{median}(A)$ the standard error of the median for set A we can write this as,

$$\text{error}(\{x\}) = \frac{1}{2}\sqrt{\text{SE}_{median}(\{x\}_{p=0})^2 + \text{SE}_{median}(\{x\}_{p=1})^2 + 2\cdot\text{SE}_{median}(\{x\}_{p=0})\cdot\text{SE}_{median}(\{x\}_{p=1})}\,, \tag{4}$$

$$\text{error}(\{y\}) = \frac{1}{2}\sqrt{\text{SE}_{median}(\{y\}_{p=0})^2 + \text{SE}_{median}(\{y\}_{p=1})^2 + 2\cdot\text{SE}_{median}(\{y\}_{p=0})\cdot\text{SE}_{median}(\{y\}_{p=1})}\,, \tag{5}$$

where,

$$\text{SE}_{median}(A) = 1.2533\frac{\sigma(A)}{\sqrt{N}}\,, \tag{6}$$

with $\sigma(A)$ being the standard deviation of the set A, and N the number of elements of the set A.
From here is important to mention that the additional step of grouping events by polarization before calculating the standard deviation can lead to lower values than expected for the total error for certain event distribution.
Given that the standard error of the median is inversely proportional to the square root of the number of events, the number of events in each segment is crucial for a precise position estimation. This implies that a higher event rate will result in a more precise position estimation for the same acquisition time t_{acq}.
For a sample that, under certain conditions, has an event rate r_{event}, the average number of events used to determine its position can be written as $N = r_{\text{event}} \cdot t_{acq}$. From this relation, since the dispersion of events would be expected to be the same for particles of similar size and shape, the key factor responsible for variations in the standard error is the number of events used to calculate the position that depends linearly with the acquisition time. This is the relation used to obtain the plot for figure 3c.
In order to validate our proposed algorithm with standard tracking techniques we used a modified version of the experimental setup to simultaneously record the motion of the particle in a CMOS camera and an EBC, see figure 3. We calibrated the pixel size of each camera using a microcalibration test target (USAF 1951, Thorlabs). To obtain the particle positions from the CMOS we use a centroid method from the OpenCV library in python. The estimated uncertainty of the centroid method is close to the pixel size, similar to the ones obtained from the EBC for frame 3 in figure 3b in the main text.
Figure 4 shows a comparison of the particle trajectory obtained from the CMOS-based centroid method and our EBC-based algorithm. The respective acquisition rates are 17.5 and 2000 fps, which explains the apparent dispersion on the EBC results. The acquisition rate of the CMOS camera is low enough so the induced modulation of the image plane is averaged out. The Pearson correlation factor between the trajectories obtained by each method (after interpolating the CMOS data to match number of points) are 0.98 and 0.97 for the x and y component, respectively.

Supplementary Methods 2: EBC pixel-to-length ratio

The pixel-to-spatial resolution (51.0 nm/pixel) for the EBC was measured using a microcalibration test target, specifically a negative USAF 1951. Being a negative test target means that the reference lines are transparent, while the background is opaque. The target is illuminated with a light source and the image is captured by the EBC similarly to the microparticles

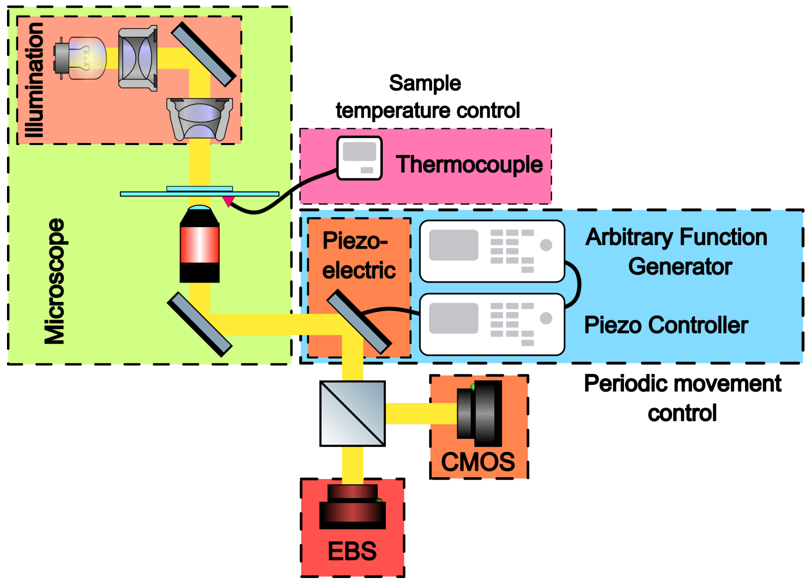

Figure 3. Modified optical system implemented to allow simultaneous recording of the particle using a CMOS camera and an EBC. A 50:50 beamsplitter is added before the EBC, and a CMOS camera is placed in the new optical path.

visualization. Since the target is a still image, the events detected by the EBC result from noise in the sensor in areas of high illumination. Events within the region of the calibration bars accumulate over time, so with a sufficiently long recording, the test target becomes visible in the event data. A frame-like representation of the recording can be found in panel a of figure 5. The list of events is converted into a density plot counting the number of events detected by each pixel, resulting in an image of the calibration bars similar to that produced by a classical camera. From this, the width of the bar in pixels can be obtained, the inclination relative to the sensor array can be compensated, and the pixel-to-spatial resolution ratio can be calculated.

References

1. Weast, R. C., Astle, M. J. & Beyer, W. H. (eds.) *CRC handbook of chemistry and physics: a ready-reference book of chemical and physical data* (CRC Press, Boca Raton, Fla, 1988), 69. ed edn.

2. Hardy, R. C. & Cottington, R. L. Viscosity of deuterium oxide and water in the range 5 to 125 C. *J. Res. Natl. Bureau Standards* **42**, 573, DOI: 10.6028/jres.042.049 (1949).

3. Swindells, I., Coe, J. R. & Godfrey, T. B. Absolute Viscosity of Water at 20° C. *J. Res. Natl. Bureau Standards* **48** (1952).

4. Lorentz, H. A. Abhandlungen über theoretische physik. *Monatshefte für Math. und Physik* **18**, A32–A32, DOI: 10.1007/BF01694241 (1907).

5. Faxén, H. Der Widerstand gegen die Bewegung einer starren Kugel in einer zähen Flüssigkeit, die zwischen zwei parallelen ebenen Wänden eingeschlossen ist. *Annalen der Physik* **373**, 89–119, DOI: 10.1002/andp.19223731003 (1922).

6. Reinhardt, M., Bruce, N. J., Kokh, D. B. & Wade, R. C. Brownian Dynamics Simulations of Proteins in the Presence of Surfaces: Long-Range Electrostatics and Mean-Field Hydrodynamics. *J. Chem. Theory Comput.* **17**, 3510–3524, DOI: 10.1021/acs.jctc.0c01312 (2021).

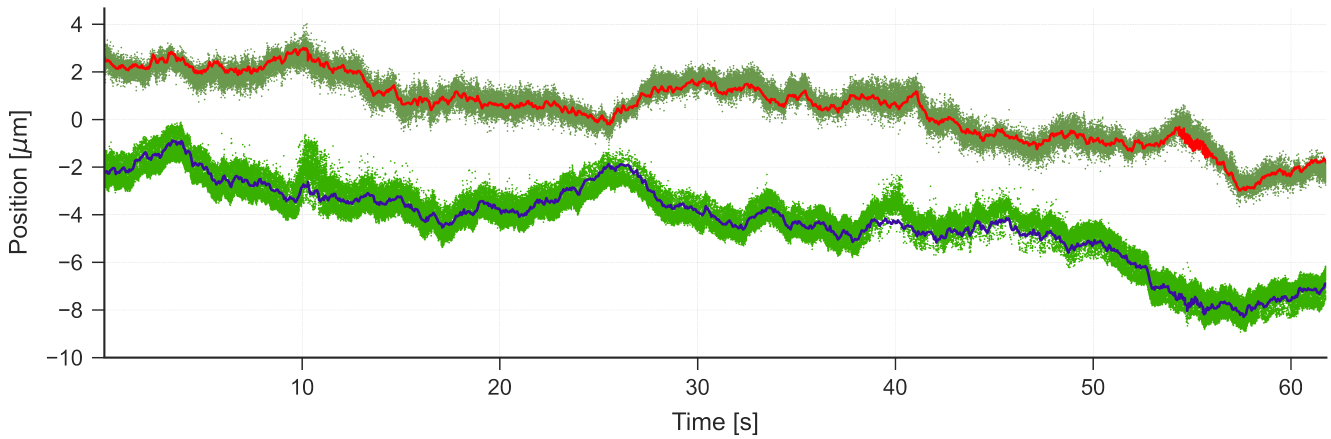

Figure 4. Comparison between the trajectories obtained with the CMOS camera and the EBC. The x- and y-position measurements from both methods are superimposed, showing similar overall behavior. The upper curves represent the x-positions, while the lower curves correspond to the y-positions. The EBC trajectories, characterized by a high density of points, are displayed as scattered points forming broader regions, while the CMOS trajectories are represented as solid lines overlaying the EBC data.

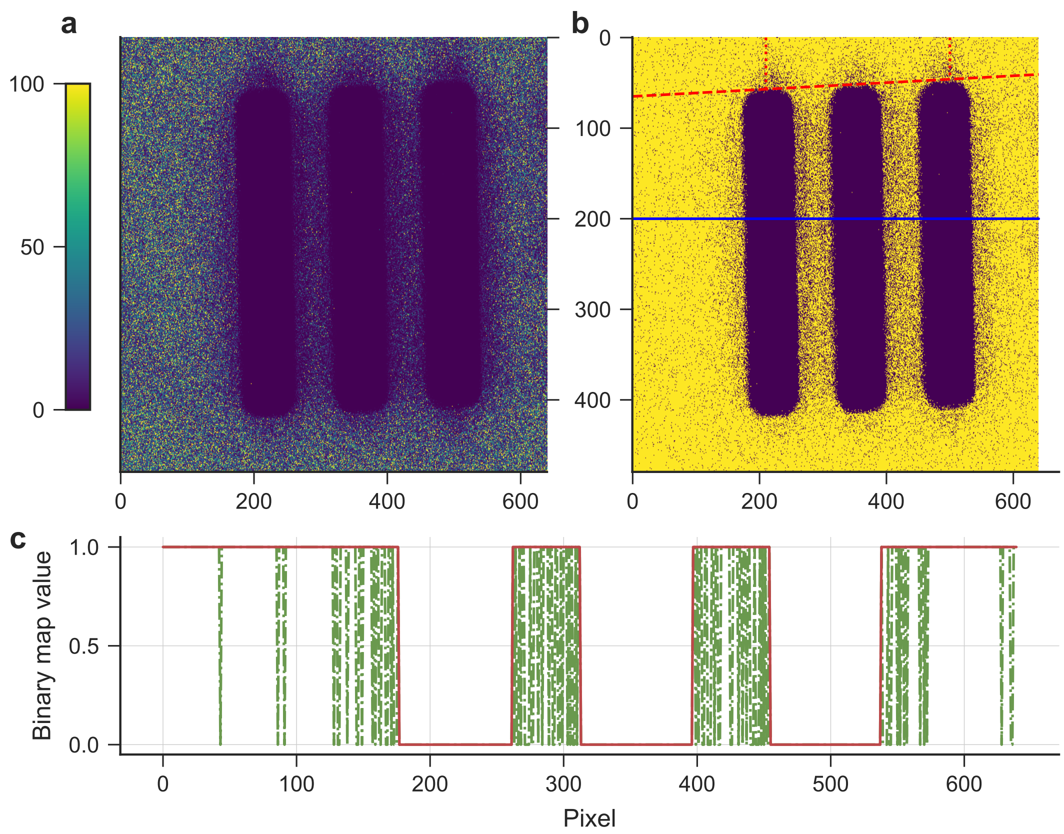

Figure 5. Steps to measure the pixel-to-spatial resolution of the EBC. (a) Colormap showing how many events were registered by each pixel in the recording of the negative test target with the EBC, with a maximum value of 100. The lines observed correspond to group 7, element 2 of the test target. (b) All pixels that detected at least one event are set to the same value. The blue solid line represents the line used to estimate the width of each line, and the red dashed lines gives the idea of how inclination is measured to then be considered in the resolution. (c) The green dashed line shows how the line obtained from panel b looks like, and the red solid line is the result after filtering isolated pixels with no events.